Monitoring of fluconazole and caspofungin activity against in vivo *Candida glabrata* biofilms by bioluminescence imaging.

Running title: *C. glabrata* biofilm eradication in animal model system

Aranka Persyn[1,2,*], Ona Rogiers[1,2,3,4,*], Matthias Brock[5], Greetje Vande Velde[6], Mohamed Lamkanfi[3,4], Ilse D. Jacobsen[7,8,9], Uwe Himmelreich[6], Katrien Lagrou[10], Patrick Van Dijck[1,2,#] & Soňa Kucharíková[1,2, †]

[1]VIB-KU Leuven Center for Microbiology, Kasteelpark Arenberg 31, B-3001 Leuven, Belgium

[2]Laboratory of Molecular Cell Biology, Institute of Botany and Microbiology, KU Leuven, Kasteelpark Arenberg 31, B-3001 Leuven, Belgium

[3]Center for Inflammation Research, VIB, Technologiepark 927, Zwijnaarde, B-9052, Belgium

[4]Department of Internal Medicine, Ghent University, Technologiepark 927, Zwijnaarde, B-9052, Belgium

[5]School of Life Sciences, University of Nottingham, University park, NG7 2RD, United Kingdom

[6]Biomedical MRI/ MoSAIC, Department of Imaging & Pathology, KU Leuven, O&N I Herestraat 49 - box 505, 3000 Leuven, Belgium

[7]Research Group Microbial Immunology, Leibniz Institute for Natural Product Research and Infection Biology, Hans Knöll Institute (HKI), Beutenbergstraße 11a, 07745 Jena, Germany

[8]Center for Sepsis Control and Care (CSCC), University Hospital Jena, Bachstraße 18, 07745 Jena, Germany

[9]Institute for Microbiology, Friedrich Schiller University, Fürstengraben 1, 07745 Jena, Germany

[10]KU Leuven, Department of Microbiology and Immunology, Laboratory of Clinical Bacteriology and Mycology, UZ Herestraat 49, 3000 Leuven, Belgium

[†]Current affiliation: University of Trnava, Faculty of Health care and Social work, Univerzitné námestie nr. 1, 918 43 Trnava, Slovakia

*These authors contributed equally to this work.

#Corresponding author

Prof. Patrick Van Dijck

KU Leuven, Laboratory of Molecular Cell Biology, VIB-KU Leuven Center for Microbiology, Institute of Botany and Microbiology, Kasteelpark Arenberg 31 - Box 2438, B-3001 Leuven-Heverlee, Belgium, Tel: +32 16 32 15 12, Fax: +32 16 32 19 79, email: patrick.vandijck@kuleuven.vib.be

Abstract

Candida glabrata can attach to various medical implants and forms thick biofilms despite its inability to switch from-yeast-to hyphae. Current in vivo *C*. *glabrata* biofilm models only provide limited information about colonization and infection and usually require animal sacrifice. To gain real-time information from individual BALB/c mice we developed a non-invasive imaging technique to visualize *C*. *glabrata* biofilms in catheter fragments that were subcutaneously implanted on the back of mice. Bioluminescent *C*. *glabrata* reporter strains (*luc*$_{OPT}$ 7/2/4 and *luc*$_{OPT}$ 8/1/4), free of auxotrophic markers, expressing a codon-optimized firefly luciferase were generated. A murine subcutaneous model was used to follow real-time in vivo biofilm formation in the presence and absence of fluconazole and caspofungin. Fungal load in biofilms was quantified by colony forming unit counts and by bioluminescence imaging (BLI). *C*. *glabrata* biofilms formed within the first 24 h, as documented by the increased number of device-associated cells and elevated bioluminescent signal compared to adhesion at the time of implant. The in vivo model allowed monitoring of the anti-biofilm activity of caspofungin against *C*. *glabrata* biofilms through bioluminescent imaging from day four after initiation of treatment. Contrarily, signals emitted from biofilms implanted in fluconazole-treated mice was similar to the light emitted from control-treated mice.

This study gives insights into real-time development of *C*. *glabrata* biofilms under in vivo conditions. BLI proved to be a dynamic, non-invasive and sensitive tool to monitor continuous biofilm formation and activity of antifungal agents against *C*. *glabrata* biofilms formed on abiotic surfaces in vivo.

Introduction

Candida glabrata is an emerging human fungal pathogen causing mucosal and deep tissue infections especially in elderly patients with a compromised immune system. Following *Candida albicans, C. glabrata* is the second most common isolated species from hospitalized patients in Europe (1). Although *C. glabrata* does not possess the ability to form true hyphae or secrete proteases, it still maintains many virulence factors, including biofilm forming capacity, which contribute to its potential to cause disease (2). The majority of life-threatening infections are associated with biofilm formation on biotic and abiotic substrates. Biofilms provide microorganisms with a shelter from external effects of therapeutics, giving them an opportunity to withstand very high concentrations of antifungal agents, for example azoles (3, 4). Because of biofilm resilience to antifungals, therapeutic approaches are very limited, often leading to surgical removal of the implant material and its subsequent replacement as sole solution. Recently, our group demonstrated that in vivo *C. glabrata* biofilms formed inside polyurethane catheter pieces implanted subcutaneously on the back of Sprague Dawley rats (5). Biofilms were composed of multilayer structures of yeast cells embedded in extracellular matrix exhibiting increased tolerance to therapeutic concentration of fluconazole. Echinocandins proved to remain active against in vivo *C. glabrata* biofilm-forming cells in this particular model (5). One disadvantage of almost all existing biofilm models is that the fungal load is traditionally analyzed *post mortem*, requiring host sacrifice. To avoid this, sensitive non-invasive techniques, such as bioluminescence imaging (BLI), provide new and often unexpected temporal and spatial information on infection development in individual animals in real time (6, 7). The monitoring of light emitted from luciferase-expressing reporter cells has been used to examine an extensive range of biomolecular functions (8). BLI has been successfully applied to monitor the development of oral

candidiasis (6, 9) and *C. albicans* dissemination after tail vein injection in mice (10-12). This technique was also employed to follow superficial and subcutaneous infections caused by *C. albicans* (12). Moreover, it was employed to study the time-dependent development of *C. albicans* biofilm formation in a subcutaneous biofilm mouse model (13).

In this study, we present the construction of an auxotrophic marker-free bioluminescent *C. glabrata* reporter strain based on a *C. glabrata*-optimized firefly luciferase integrated into the *HIS1* locus using *HIS1* as selectable marker. This allowed us to study biofilm development in real-time by use of BLI in a mouse subcutaneous model system. It furthermore allowed us to monitor efficacy of fluconazole and caspofungin treatment in vivo and can thereby contribute to implementation of the 3Rs (replacement, reduction and refinement of animal testing) in therapeutic experiments.

Results

In vitro characterization of bioluminescent strains

C. glabrata reporter strains *luc*$_{OPT}$ 7/2/4 and *luc*$_{OPT}$ 8/1/4 were generated via integration of a *C. glabrata*-optimized firefly luciferase into the *HIS1* locus using *HIS1* as selectable marker. To ensure that *C. glabrata luc*$_{OPT}$ 7/2/4 and *luc*$_{OPT}$ 8/1/4 produced substantial bioluminescence and that luciferase expression did not affect growth rates, transformants were tested in series of in vitro experiments. We did not observe any changes in growth rates between reporter strains and WT in RPMI 1640, pH 7.0 and YPD medium at 37 °C (Figure S1). Additionally, we prepared 10-fold dilution series of WT and bioluminescent strains to detect the signal. Signals from reporter strains correlated (Spearman r=0.993, n=24, p<0.0001) well with the number of cells with a detection limit of about 100 cells per well (Figure S1).

In vitro *Candida glabrata* adhesion and biofilm formation monitored by BLI

To evaluate the potential use of BLI in vitro to study fungal adhesion (90 min after inoculation) and biofilm formation (after 2 days), we inoculated *C. glabrata* strains on the serum-coated bottom of 96-well polystyrene plates, which represents a very simple biofilm system. The bioluminescent signal acquired from the reporter strains was significantly higher compared to the WT (Figure 1A, C). A parallel XTT assay showed a significant increase in metabolic activity for all biofilm-forming cells after 2 days (Figure 1B). The BLI signal intensity from biofilms formed by luciferase-expressing strains on polyurethane catheters increased significantly compared to the signal determined from the WT strain (Figure 1D, F). The number of cfu was significantly higher during biofilm formation in comparison to adhesion (Figure 1E), which is in agreement with the BLI signal measurements. To determine whether BLI can accurately measure kinetics of *C. glabrata* biofilm formation, we quantified bioluminescence and cfu quantification after 90 min (adhesion period), 1, 2, 5 and 7 days. At each imaging time point, the BLI signal retrieved from reporter strain *C. glabrata* luc_{OPT} 7/2/4 cells was significantly higher compared to the signal emitted from the WT strain (Figure 2A, C). The number of fungal cells significantly increased between adhesion and the first 24 h of biofilm formation (Figure 2B). At later time points of biofilm formation, the BLI signal and the amount of cfu remained stable. In addition, we show that this reporter strain allows accurate in vitro biofilm quantification, as cfu and bioluminescence correlated well (Spearman r=0.7027, n=27, $p<0.0001$). Taken together, these results indicate that BLI represents a sensitive tool to study in vitro *C. glabrata* adherence and biofilm formation on abiotic surfaces.

In vivo BLI of *Candida glabrata* biofilms developed in a subcutaneous mouse model

Biofilm formation can impose serious medical problems in immunocompromised patients. First, we assessed the role of immunosuppression on *C. glabrata* biofilm and on dissemination into the surrounding tissue. One group of mice was treated with dexamethasone (0.4 mg/L) in the drinking water, whereas the second group remained immunocompetent. Our preliminary experiment displayed no major differences in the number of cfu after devices were explanted from immunocompromised and immunocompetent mice (Figure S2 A). Similarly, the number of *C. glabrata* cells quantified from tissue surrounding catheters was almost identical (Figure S2 B). As no significant difference was observed among both groups we continued our experiments in immunocompetent mice. Moreover, fungal cells did not disseminate into any vital organ of immunocompromised or immunocompetent mice as no cfu were retrieved from kidneys, liver nor spleen after homogenization (data not shown).

In this model, catheters infected with *C. glabrata* WT cells and luc_{OPT} 7/2/4 expressing strain were implanted subcutaneously on the left and right side, respectively of the lower back of mice (Figure 3A). In vivo imaging was performed after catheter implant and continued on day 1, 5 and 7 (Figure 3A). At every imaging time point 3 mice were sacrificed and explanted catheters were used for ex vivo quantification. A significant BLI signal was detected only from *C. glabrata* luc_{OPT} 7/2/4 biofilm-forming cells, where it increased significantly over time (Figure 3A, B). The quantification of cfu documented with the BLI signal in parallel was significantly higher between adhesion (90 min) and 1st day of biofilm maturation (Figure 3C). Moreover, the number of biofilm-forming cells and bioluminescent signal retrieved from *C. glabrata* luc_{OPT} 7/2/4 correlated well (Spearman r=0.7576, n=10, p<0.0149) (Figure 3A, B). These findings indicate that BLI can be used for continuous detection and quantification of in vivo *C. glabrata* biofilm formation.

175 **In vivo BLI of fluconazole and caspofungin activity against *C. glabrata* biofilms**

176 Prior to in vivo experiments, we performed few tests to determine the efficacy of an azole
177 fluconazole and an echinocandin caspofungin on free-living cells and in vitro biofilms. *C*.
178 *glabrata* planktonic cells showed decreased susceptibility to fluconazole (MIC_{50} ranging
179 from 8 - 16 μg/ml), whereas all strains were susceptible to caspofungin (0.0625 mg/L). In
180 vitro *C*. *glabrata* biofilms did not respond to therapy with fluconazole (>64 mg/L), while
181 caspofungin (0.25 mg/l - 0.5 mg/L) significantly decreased the number of *C*. *glabrata*
182 biofilm-forming cells of all strains tested (Figure S3). Further, we evaluated the activity of
183 fluconazole (125 mg/kg of body weight/day) and caspofungin (10 mg/kg of body weight/day)
184 against in vivo *C*. *glabrata* biofilms. Daily in vivo imaging and the number of cfu retrieved
185 from catheters ex vivo on day 9 revealed that fluconazole was not active against *C*. *glabrata*
186 biofilm-forming cells (Figure 4A, B, C, D). In contrast, the signal detected in mice treated
187 with caspofungin significantly decreased from day 4 of treatment until day 7 (Figure 4A, B).
188 Furthermore, treatment with caspofungin resulted in significantly decreased number of cfu
189 recovered from polyurethane devices ex vivo (Figure 4C, D). In conclusion, these data
190 support the use of BLI to demonstrate activities of antifungal agents against biofilms under in
191 vivo conditions.

192

193 **Discussion**

194 Usage of indwelling medical devices has become indispensable to medical care.
195 Unfortunately, the increased risk of biofilm related infections in hospitalized patients is
196 associated with the use of these devices. One of the key challenges in biofilm research is the
197 development of in vivo models that allow assessment of the efficacy of existing or novel
198 therapeutics. So far, only a few in vitro *C*. *glabrata* biofilm model systems have been

introduced to elucidate the different stages of biofilm, its architecture and response to antifungal treatment (2). However, these models do not take the host immune system and changes at the host site of infection into consideration, which are crucial during infections in humans. Up to date, in vivo *C. glabrata* biofilms have been studied inside central venous catheters as described by Nett *et al*. (14). Recently, in vivo *C. glabrata* biofilms have been established subcutaneously in immunocompromised Sprague Dawley rats (5). In this study we established an in vivo *C. glabrata* infection model that mimics non-bloodstream biofilm-associated infections in immunocompetent mice. This model is of interest given the frequent development of such biofilms in endotracheal tubes, intracardiac prosthetics and prosthetic joints (15). Our flow cytometry experiments (data not shown) displayed a trend towards more neutrophil recruitment in the subcutaneous area surrounding catheter pieces 72 h post-surgery in animals carrying *C. glabrata*-infected catheters compared to non-infected devices. These findings suggest that the host immune system is triggered upon *C. glabrata* infection however that the predominant innate immune response is likely not driven solely by neutrophils. Further research elucidating the specific innate immune response towards these biofilms has to be conducted. Translation of the originally developed rat model to mice improved the cost-efficiency of in vivo experiments and presents potential to study biofilm formation in different transgenic mice allowing us to discover different host factors that may affect biofilm development.

In the majority of animal experiments, the number of cfu's is determined post-mortem which requires a large number of animals in order to perform time-course experiments. This is also the case if one wants to study the effect of antifungals on catheter-associated biofilm infections in animals. Because of this, we searched for an alternative tool which allowed us to study the development of infection repeatedly in the same animal. Bioluminescence imaging (BLI) has been previously described as a sensitive, reliable and non-invasive technique to

224 follow systemic candidiasis caused by *C. albicans* and its dissemination into kidneys (10-12).
225 Additionally, BLI has been applied to study subcutaneous *C. albicans* infections (10) and
226 vulvovaginal candidiasis (11). It was used to monitor *C. albicans* biofilm formation in a
227 subcutaneous catheter mouse model (13). In that particular scenario, *Gaussia princeps*
228 luciferase was expressed on the cell wall (12) and emitted light upon contact with the
229 substrate coelenterazine, whereby light emission correlated with cfu (13). Gabrielli *et al.*
230 (16), used *C. albicans* strains with extracellularly expressed *G. princeps* luciferace to study
231 development of oropharyngeal candidiasis. They found that in vivo BLI was more reliable
232 than cfu counts detecting early infection in the oral cavity of the host. Very recently, red-
233 shifted firefly luciferase has been introduced to test the fate of *C. albicans* in different animal
234 models (17). In our study, the use of firefly luciferase is known for its glow-type
235 bioluminescence over a period of time and therefore, is advantageous in comparison with
236 other reporter systems (18). *Renilla* luciferase and beetle reporter systems have been used to
237 study eukaryotes. In the case of bacteria it is advantageous to use luminescent reporters based
238 on the lux operon with intracellular expression of luciferase (6). Furthermore, the strains
239 generated here are otherwise not auxotrophic and show no altered phenotype when compared
240 to the parental WT. We have clearly demonstrated that BLI is sensitive and a powerful tool to
241 study long-term infection development on abiotic surfaces within living animals.

242 It is known that the extracellular matrix serves as a protective barrier allowing
243 microorganisms to withstand high concentrations of antimicrobial agents. Treatment of *C.*
244 *glabrata* can be especially challenging because of its acquired resistance to the *"gold-*
245 *standard"* antimycotic fluconazole (4). In our study, daily administration of fluconazole (125
246 mg/kg of body weight/day) for 7 days did not cause any significant decline in the number of
247 *C. glabrata* catheter-associated cells as comparable BLI and cfu. However, daily
248 administration of caspofungin (10 mg/kg of body weight/day) significantly decreased the

number of cfu retrieved from implanted catheters in comparison with saline-treated animals. Remarkably, daily monitoring of animals resulted in decreased signal from day 4 in caspofungin-treated animals. These studies are in agreement with our previous fluconazole and caspofungin efficacy testing in a rat model (5). Moreover, we (19) displayed that fluconazole failed its efficacy on *C. albicans* biofilms, whereas caspofungin showed very good activity to treat device-associated infections in the subcutaneous mouse model.

In conclusion, bioluminescence imaging is a reliable and non-invasive method not only to visualize but also to quantify fungal biofilms. Even more importantly, this technique is cost effective offering the capability to study the activity of novel or existing antimicrobial agents over the course of time avoiding animal sacrifice at each time point. The model presented in this study combined with BLI can be easily used by other researchers to exploit the role of the host immune system in infection when using different knockout mice, to study host-pathogen interactions using different *C. glabrata* strains, as well as for rapid screening during early drug discovery.

Materials and methods

Ethics

All animal experiments were performed in accordance with the KU Leuven animal care guidelines and were approved by the Ethical Committee of the KU Leuven (project number P090/2013). All animals were given a standard *ad libitum* diet and housed at random with 4 animals in filter-top cages in a dedicated animal room where temperature, light and humidity was regulated.

Generation of *C. glabrata* histidine auxotrophic mutants

All oligonucleotides used in this study are described in Supplementary Table 1. For generation of a histidine auxotrophic mutant of *C. glabrata* ATCC2001 (WT) the *HIS1* locus was selected for gene deletion. A 750 bp promoter region (P1 + P2) and a 693 bp downstream region (P3 + P4) of the *HIS1* gene were amplified from *C. glabrata* genomic DNA. Oligonucleotides P1 and P4 contained overlapping sequences to the *Bam*HI restricted pUC19 vector. Oligonucleotides P2 and P3 contained flanking sequences to the nourseothricin resistance cassette that was amplified with oligonucleotides P5 and P6 from plasmid pJK863 (20). Primer P5 contained an overlap to the upstream and P6 to the downstream flanking region of the *HIS1* gene. PCR reactions were performed with Phusion Hot Start II polymerase (Thermo) and PCR fragments were gel purified using the GeneJet Gel purification kit (Thermo). All fragments were mixed with the *Bam*HI restricted pUC19 plasmid and assembled by in vitro recombination using the InFusion HD cloning kit (Takara/Clonetech). After transformation of *E. coli* DH5α cells, oligonucleotides P1 + P7 and P4 + P8 were used to screen colonies for correct plasmid assembly. Plasmid DNA was isolated, restricted with *Kpn*I and used for electroporation of *C. glabrata* WT cells (21). Transformants were regenerated on YPD medium with 200 µg/mL nourseothricin. Individual colonies were tested for histidine auxotrophy. Integration of the deletion construct into the *HIS1* locus was confirmed by diagnostic PCR with oligonucleotides P7 + P9. The deletion mutants Δ2/4 and Δ2/12 were used in downstream experiments for generation of bioluminescent strains.

Generation and characterization of luciferase expressing *C. glabrata* strains

A codon-optimized synthetic firefly luciferase gene adapted to the codon usage of *C. glabrata* was used for generation of bioluminescent *C. glabrata* strains. To ensure constitutive gene expression, the promoter of the enolase gene (p*ENO1*) was selected. The

enolase promoter was amplified with oligonucleotides P10 + P11 from genomic DNA of WT and ligated into the *Nde*I-site of the luciferase gene containing plasmid pUC57. The *ENO1* promoter in combination with the luciferase gene was amplified with oligonucleotides P12 + P13, whereby P12 contained an overhang to a short terminator region of the *HIS1* gene and P13 an overhang to a downstream region of the *HIS1* gene. To integrate the luciferase construct into the original *HIS1* locus of the Δ*HIS1* strains, the *HIS1* gene with 720 bp promoter region and a short 60 bp terminator sequence were amplified from genomic DNA of WT with oligonucleotides P14 + P15. Oligonucleotide P14 contained an overhang to the *Bam*HI site of the pUC19 plasmid and P15 an overhang to the *ENO1* promoter. Finally, to enable a homologous integration into the *HIS1* locus, a 668 bp downstream region of the *HIS1* gene was amplified from *C*. *glabrata* genomic DNA with oligonucleotides P16 and P17, whereby P16 overlapped with the 3'-end of the luciferase and P17 with the *Bam*HI restricted puC19 vector. All PCR fragments were gel purified and mixed with the *Bam*HI restricted puC19 vector for in vitro recombination using the InFusion HD cloning kit. *E*. *coli* DH5α was transformed with the reaction mixture and correct plasmids were identified by colony PCR using oligonucleotides P18 + P19 for the fusion of the luciferase cassette with the *HIS1* gene and P20 +P21 for the combination of the luciferase gene with the *HIS1* downstream region. Correctly assembled plasmids were purified and the transformation cassette was excised from the pUC19 backbone by *Bam*HI restriction and used for transformation of *C*. *glabrata HIS1* deletion mutants using histidine prototrophy as selection marker. Transformants were regenerated on yeast nitrogen base (YNB) with ammonium but w/o amino acids and niacin as supplement. Transformants were pre-screened for loss of nourseothricin resistance, which was expected by homologous integration of the reporter cassette into the original *HIS1* locus of *HIS1* deletion mutants. Integration of the cassette into the correct locus was additionally confirmed by diagnostic PCR using oligonucleotides P9 +

P22. Finally, transformants were streaked on YNB agar plates containing 0.4 mM D-luciferin and analyzed for bioluminescence using an IVIS 100 system (Perkin Elmer). Two independent transformants, namely *C. glabrata* luc_{OPT} 7/2/4 and luc_{OPT} 8/1/4 producing similar signal intensities were selected for further work. An overview of the strains used in this study is provided in Supplementary Table 2.

All strains were grown on YPD (1% yeast extract, 2% peptone, 2% glucose) agar plates at 30 °C. *C. glabrata* planktonic cultures were incubated in liquid YPD medium for 72 h at 30 °C (stationary phase). The growth of planktonic cells was followed by BioscreenC (Labsystems) at 30 °C and 37 °C under continuous shaking for 24 hours and measurements were taken every 30 min.

In vivo *C. glabrata* biofilm formation in a murine subcutaneous biofilm model

We translated a rat subcutaneous biofilm model (5) to specific pathogen-free immunocompetent BALB/c mice (6-8 weeks old, 20 g). *C. glabrata* (1×10^6 cells/mL) attached onto the surface of serum-coated polyurethane catheter pieces during in vitro adhesion (90 min, 37°C) followed by a washing step with PBS. Mice were anesthetized as previously described (5). In order to compare bioluminescence from the WT control strain and the bioluminescent strain in a single animal, two small incisions were made, one on the left and one on the right side of the back of a mouse, as previously demonstrated (22). Three catheter pieces seeded with WT were implanted on the left and 3 catheters infected with bioluminescent strain were inserted on the right side of the back. For catheter explant, animals were sacrificed by cervical dislocation. Catheter fragments were removed, washed twice with PBS and placed to microcentrifuge tubes containing PBS. Devices were sonicated, vigorously vortexed and plated to enumerate the number of colony-forming units (cfu).

Dissemination of *C. glabrata* cells from biofilms into the kidneys, liver, spleen and the tissue surrounding the catheter pieces was examined after 48 and 144 h of biofilm formation.

In vivo BLI

Isoflurane anesthesia and the BLI procedure were performed as described before (13, 22). Prior to BLI, fresh D-luciferin solution (33.3 mg/mL) was dissolved in sterile saline (0.9 % NaCl). A photograph was taken to ensure that the animals are in the desired position for imaging. Subsequently, 100 µL of the D-luciferin substrate was injected subcutaneously at both sides of the back, at the regions surrounding the implanted catheter pieces. During substrate injection, animals were kept anaesthetized through a nose cone providing gas anesthesia. Consecutive series of scans were acquired at 60 s exposure time (medium binning) until the maximum signal was reached (around 15 min after injection). Rectangular region of interests (ROIs) were drawn around each trio of catheters and reported as photon flux per second ($p\ s^{-1}$). Background BLI signal was measured by using the same ROI after injecting D-luciferin subcutaneously on the upper back of the mouse where no catheters were implanted.

In vivo antifungal treatment

Stock solution of fluconazole (Sigma Aldrich, USA) was dissolved in sterile water, whereas caspofungin was prepared in pure DMSO. Intraperitoneal administration of fluconazole (125 mg/kg of body weight/day) and caspofungin (10 mg/kg of body weight/day) was initiated 24 h post implant. Solutions for injection were prepared in sterile saline and administered intraperitoneally once daily for 7 days. In case of caspofungin the concentration of DMSO

used for the injection was 0.5%. Control group of mice was injected with sterile saline.

Additional materials and methods are described in Supplementary file.

Acknowledgement

We thank Celia Lobo Romero for her excellent technical assistance during in vitro and in vivo experimental procedures. We express our gratitude to Tinne Buelens and Ann Van Santvoort for their technical assistance during animal experiments and bioluminescence imaging, performed at the Molecular Small Animal Imaging Facility (MoSAIC) of KU Leuven. We acknowledge Nico Vangoethem for his help with figures and tables. This work was funded by the Merck Investigator Studies Program number 40312 awarded to P.V.D; by a Research Grant (2013) by the European Society of Clinical Microbiology and Infectious Diseases (ESCMID) awarded to S.K and by the Fund for Scientific Research Flanders (FWO research community on biofilms WO.009.16N). S.K. is a postdoctoral fellow of the Fund for Scientific Research Flanders (FWO). S.K. was supported also by a postdoctoral grant of the KU Leuven (PDMK 11/089). O.R. is supported by Strategic Basic Research (SB) grant Research Foundation-Flanders (FWO) and grant number 1S55817N.

References

1. Kullberg BJ, Arendrup MC. 2015. Invasive Candidiasis. N Engl J Med 373:1445-1456.

2. Rodrigues CF, Rodrigues ME, Silva S, Henriques M. 2017. *Candida glabrata* biofilms: how far have we come? J Fungi 3:pii: E11.

3. d' Enfert C, Janbon G. 2016. Biofilm formation in *Candida glabrata*: What have we learnt from functional genomics approaches? FEMS Yeast Res 16:fov111.

4. Perlin DS, Rautemaa-Richardson R, Alastruey-Izquierdo A. 2017. The global problem of antifungal resistance: prevalence, mechanisms, and management. Lancet Infect Dis 17:e383-e392.

5. Kucharíková S, Neirinck B, Sharma N, Vleugels J, Lagrou K, Van Dijck P. 2015. *In vivo Candida glabrata* biofilm development on foreign bodies in a rat subcutaneous model. J Antimicrob Chemother 70:846-856.

6. Brock M. 2012. Application of bioluminescence imaging for in vivo monitoring of fungal infections. Int J Microbiol 2012:956794.

7. Vecchiarelli A, d' Enfert C. 2012. Shedding natural light on fungal infections. Virulence 3:15-17.

8. Close DM, Xu T, Sayler GS, Ripp S. 2011. *In vivo* bioluminescence imaging (BLI): noninvasive visualization and interrogation of biological processes in living animals. Sensors (Basel) 11:180-206.

9. Mosci P, Pericolini E, Gabrielli E, Kenno S, Perito S, Bistoni F, d' Enfert C, Vecchiarelli A. 2013. A novel bioluminescence mouse model for monitoring oropharyngeal candidiasis in mice. Virulence 4:250-254.

412 10. Jacobsen ID, Lüttich A, Kurzai O, Hube B, Brock M. 2014. In vivo imaging of
413 disseminated murine *Candida albicans* infection reveals unexpected host sites of fungal
414 persistence during antifungal therapy. J Antimicrob Chemother 69:2785-2796.
415 11. Doyle TC, Nawotka KA, Kawahara CB, Francis KP, Contag PR. 2006. Visualizing
416 fungal infections in living mice using bioluminescent pathogenic *Candida albicans* strains
417 transformed with the firefly luciferase gene. Microb Pathog 40:82-90.
418 12. Enjalbert B, Rachini A, Vediyappan G, Pietrella D, Spaccapelo R, Vecchiarelli A,
419 Brown AJ, d' Enfert C. 2009. A multifunctional synthetic *Gaussia princeps* luciferase
420 reporter for live imaging of *Candida albicans* infections. Infect Immun 77:4847-4858.
421 13. Vande Velde G, Kucharíková S, Schrevens S, Himmelreich U, Van Dijck P. 2014.
422 Towards non-invasive monitoring of pathogen-host interactions during *Candida albicans*
423 biofilm formation using *in vivo* bioluminescence. Cell Microbiol 16:115-130.
424 14. Nett J, Lincoln L, Marchillo K, Andes D. 2007. Beta -1,3 glucan as a test for central
425 venous catheter biofilm infection. J Infect Dis 195:1705-1712.
426 15. Ramage G, Martinez JP, Lopez-Ribot JL. 2006. Candida biofilms on implanted
427 biomaterials: a clinically significant problem. FEMS Yeast Res 6:979-86.
428 16. Gabrielli E, Roselletti E, Luciano E, Sabbatini S, Mosci P, Pericolini E. 2015.
429 Comparison between bioluminescence imaging technique and CFU count for the study of
430 oropharyngeal candidiasis in mice. Cytometry 87:428-436.
431 17. Dorsaz S, Coste AT, Sanglard D. 2017. Red-shifted firefly luciferase optimized for
432 *Candida albicans* in vivo bioluminescence imaging. Front Microbiol 8:1478.
433 18. Badr CE. 2014. Bioluminescence imaging: basics and practical limitations. Methods
434 Mol Biol 1098:1-18.

19. Vande Velde G, Kuchariková S, Van Dijck P, Himmelreich U. 2018. Bioluminescence imaging increases in vivo screening efficiency for antifungal activity against device-associated *Candida albicans* biofilms. Int J Antimicrob Agents 52:42-51.

20. Shen J, Guo W, Köhler JR. 2005. *CaNAT1*, a heterologous dominant selectable marker for transformation of *Candida albicans* and other pathogenic *candida* species. Infect Immun 73:1239-1242.

21. Schwarzmüller T, Ma B, Hiller E, Istel F, Tscherner M, Brunke S, Ames L, Firon A, Green B, Cabral V, Marcet-Houben M, Jacobsen ID, Quintin J, Seider K, Frohner IE, Glaser W, Jungwirth H, Bachellier-Bassi S, Chauvel M, Zeidler U, Ferrandon D, Gabaldón T, Hube B, d' Enfert C, Rupp S, Cormack BP, Haynes K, Kuchler K. 2014. Systematic phenotyping of a large-scale *Candida glabrata* deletion collection reveals novel antifungal tolerance genes. PloS Pathog 10:e1004211.

22. Kucharíková S, Vande Velde G, Himmelreich U, Van Dijck P. 2015. *Candida albicans* biofilm development on medically-relevant foreign bodies in a mouse subcutaneous model followed by bioluminescence imaging. J Vis Exp (95):52239. doi: 10.3791/52239.

Figure legends:

Figure 1. In vitro BLI of *Candida glabrata* biofilm formation on 96 well plate and inside polyurethane catheters

(A) Bioluminescence signal intensity and **(B)** XTT data measurements were obtained after adherence (90 min, black columns, n = 18 wells or devices per strain) and biofilm formation (48 h, white columns, n = 18 wells or catheters per strain) by *C. glabrata* ATCC 2001 (WT), *C. glabrata* luc_{OPT} 7/2/4 and luc_{OPT} 8/1/4 in 96-well plate. **(C)** A characteristic bioluminescent image of 2 days-old biofilm formed on the surface of a 96-well plate. **(D)** Measurements of BLI signal and **(E)** colony forming unit counts (cfu) from *C. glabrata* adhered cells (90 min, black columns) and biofilms formed (48 h, white columns) inside catheters. **(F)** A typical picture of BLI acquired after 2 days of biofilm formation inside polyurethane fragments. Statistical analyses were performed using Two-way ANOVA with post-hoc Tukey HSD test. Differences were considered significant at $*p \leq 0.05$. Error bars indicate SD of replicate samples.

Figure 2. In vitro BLI of *Candida glabrata* ATCC 2001 (WT) and *C. glabrata* luc_{OPT} 7/2/4 biofilm formation inside polyurethane catheters over time

(A) Bioluminescent signal intensity acquired at different time points (adhesion, 1, 2, 5 and 7 days) of *C. glabrata* ATCC 2001 (WT, black columns) and *C. glabrata* luc_{OPT} 7/2/4 (white columns) biofilm development inside catheters. **(B)** BLI was accompanied with colony forming unit counts (cfu) after adherence and 1, 2, 5 and 7 days of in vitro biofilm formation inside polyurethane devices (n = 18 devices per strain and time point). **(C)** A BLI signal retrieved after adhesion (90 min) and later stages of biofilm formation. Two-way ANOVA

with post-hoc Tukey HSD test was used to perform statistical analyses. Differences were considered significant at *$p \leq 0.05$ and error bars indicate SD of replicate samples.

Figure 3. In vivo *Candida glabrata* ATCC 2001 (WT) and *Candida glabrata luc*$_{OPT}$ 7/2/4 biofilm formation studied by longitudinal BLI

(A) In vivo BLI of *C. glabrata* biofilm formation after implant (90 min, period of adhesion) and 1, 5 and 7 days of biofilm formation. Three polyurethane devices infected with *C. glabrata* ATCC2001 (WT) strain were implanted on left side of the back, whereas 3 devices challenged with *luc*$_{OPT}$ 7/2/4 were inserted on the ride side of the back of the animal. **(B)** Quantification of bioluminescence signal intensity acquired at different time points (adhesion, 1, 5 and 7 days, n=6 animals per time point, except for a group with non-infected catheters with n=1) of non-infected devices (black columns), *C. glabrata* ATCC 2001 (grey columns) and *C. glabrata luc*$_{OPT}$ 7/2/4 (white columns) biofilm formation. **(C)** Colony forming unit counts (cfu) retrieved from catheters infected with *C. glabrata* ATCC2001 (black columns) and with *C. glabrata luc*$_{OPT}$ 7/2/4 (white columns) after adhesion and 1, 5 and 7 days of in vitro biofilm formation inside polyurethane devices. **(C)** A BLI signal intensity retrieved after adhesion (90 min) and later stages of biofilm formation. Statistical analyses were performed using Two-way ANOVA with post-hoc Tukey HSD test. Differences were considered significant at *$p \leq 0.05$ and error bars indicate SD of replicate samples.

Figure 4. BLI of fluconazole (FLC) and caspofungin (CAS) efficacy against in vivo *Candida glabrata* ATCC 2001 (WT) and *Candida glabrata luc*$_{OPT}$ 7/2/4 biofilm-associated infections

(A) Representative images of a signal acquired from *Candida glabrata* ATCC 2001 (WT, 3 devices implanted on the left side of the back of mice) and *C. glabrata* luc_{OPT} 7/2/4 (3 catheters inserted on the right side of the back of a host) biofilms. Biofilms were formed for 24 h and afterwards treatment with fluconazole (125 mg/kg of body weight/day, n=4) and caspofungin (10 mg/kg of body weight/day, n=4) was initiated. Drugs were administered once daily for 7 days. Control-treated group of animals (n=4) was injected with sterile saline. **(B)** Quantification of BLI signal intensity, which started to decrease 4 days after animal treatment with caspofungin. Data show an average ± SEM of a BLI signal acquired from catheters implanted in animals treated with fluconazole or caspofungin on different days. **(C)** *C. glabrata* ATCC 2001 and **(D)** *C. glabrata* luc_{OPT} 7/2/4 colony forming unit (cfu) counts retrieved from individual catheters after biofilm formation. Each symbol represents the Log10 colony forming units (cfu) ± SEM of saline-treated (control) and treated fungal cells retrieved from catheter pieces from individual mice. The bar represents the average Log10 cfu ± SEM of the number of fungal cells retrieved from a drug-free and from a treated group of animals. Two-way ANOVA with post-hoc Tukey HSD test was used to calculate statistical significance, when $*p \leq 0.05$.

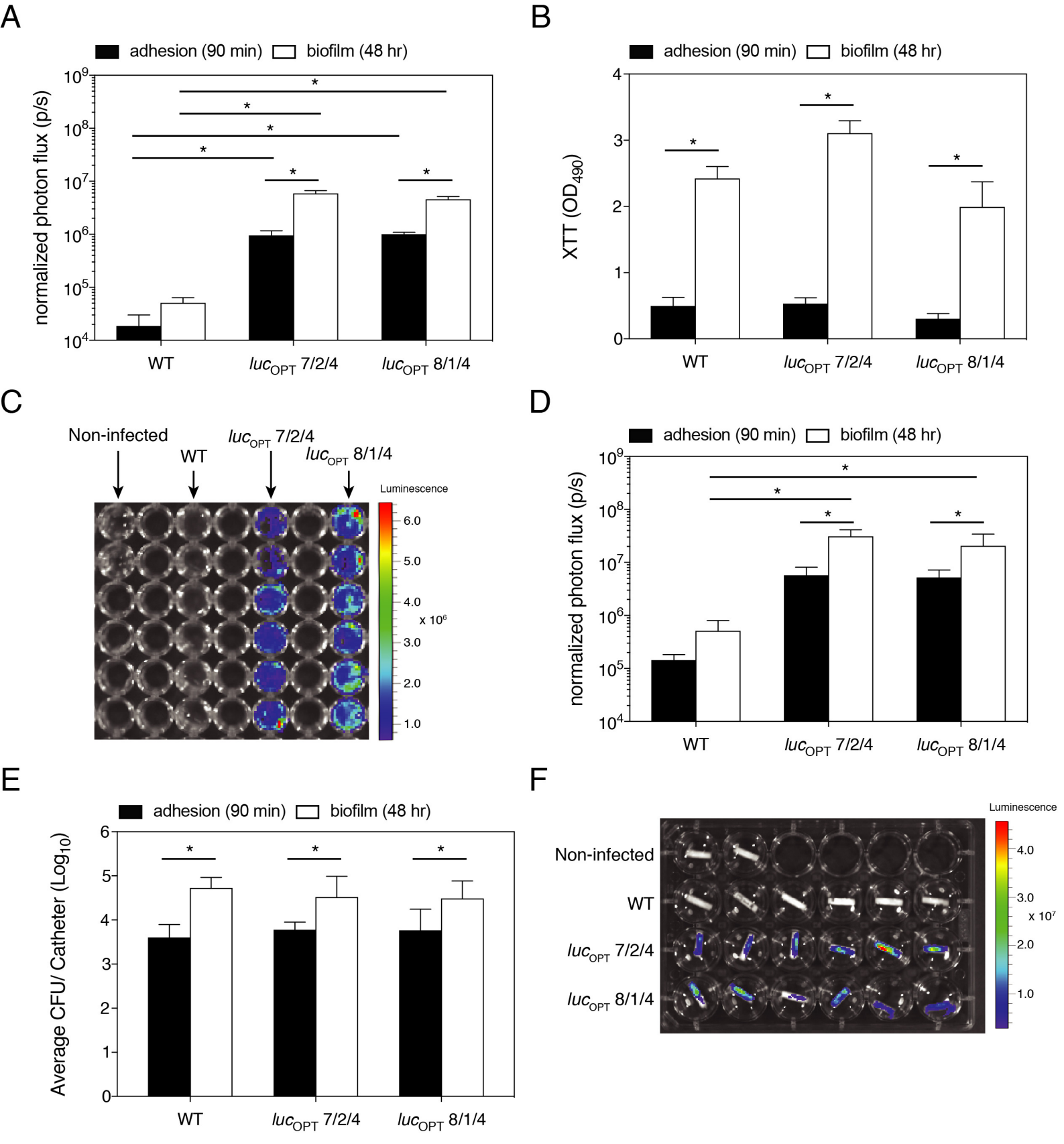
A
adhesion (90 min)
biofilm (48 hr)
normalized photon flux (p/s)
WT
luc_OPT 7/2/4
luc_OPT 8/1/4
B
XTT (OD490)
C
Non-infected
Luminescence
x 10^6
D
E
Average CFU/ Catheter (Log10)
F
Luminescence
x 10^7

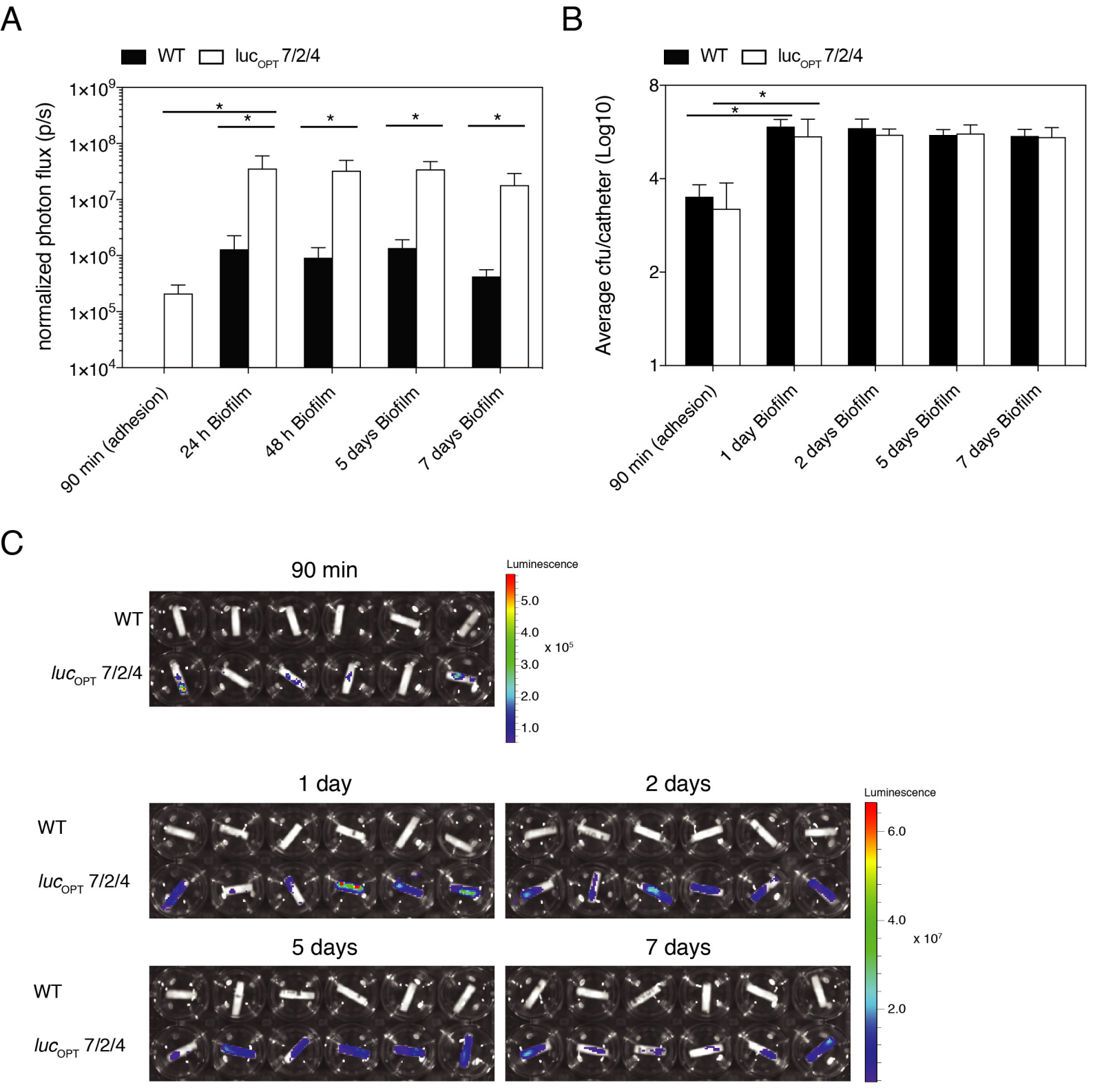
A
WT
luc$_{OPT}$ 7/2/4
normalized photon flux (p/s)
1×10^9
1×10^8
1×10^7
1×10^6
1×10^5
1×10^4
*
90 min (adhesion)
24 h Biofilm
48 h Biofilm
5 days Biofilm
7 days Biofilm
B
WT
luc$_{OPT}$ 7/2/4
Average cfu/catheter (Log10)
8
4
2
1
*
90 min (adhesion)
1 day Biofilm
2 days Biofilm
5 days Biofilm
7 days Biofilm
C
90 min
WT
luc$_{OPT}$ 7/2/4
Luminescence
5.0
4.0
x 10^5
3.0
2.0
1.0
1 day
2 days
WT
luc$_{OPT}$ 7/2/4
Luminescence
6.0
4.0
x 10^7
2.0
5 days
7 days
WT
luc$_{OPT}$ 7/2/4

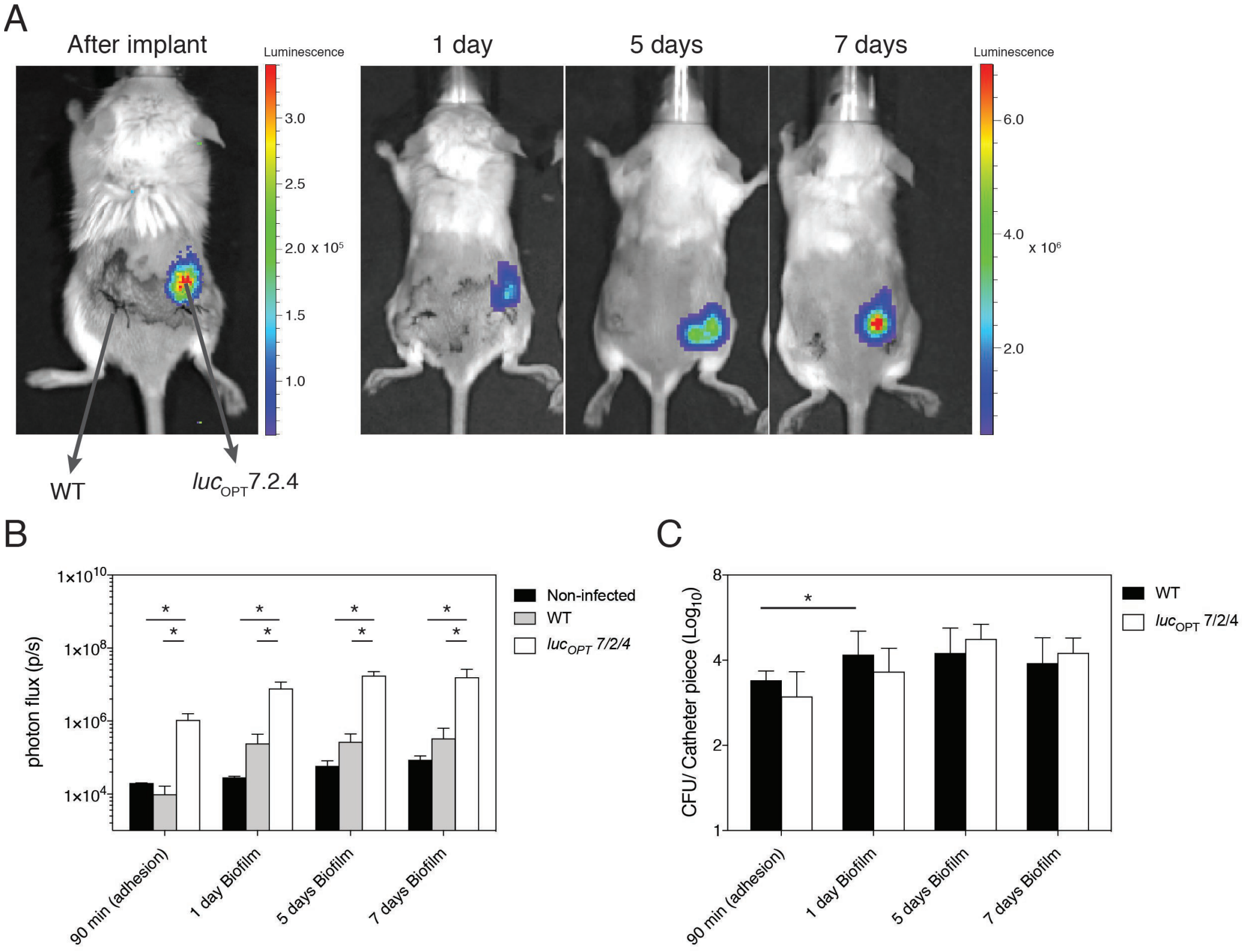
A
After implant
1 day
5 days
7 days
Luminescence
3.0
2.5
2.0 x 10^5
1.5
1.0
Luminescence
6.0
4.0
x 10^6
2.0
WT
luc_OPT7.2.4
B
photon flux (p/s)
1x10^10
1x10^8
1x10^6
1x10^4
Non-infected
WT
luc_OPT 7/2/4
90 min (adhesion)
1 day Biofilm
5 days Biofilm
7 days Biofilm
C
CFU/ Catheter piece (Log10)
8
4
2
1
WT
luc_OPT 7/2/4
90 min (adhesion)
1 day Biofilm
5 days Biofilm
7 days Biofilm

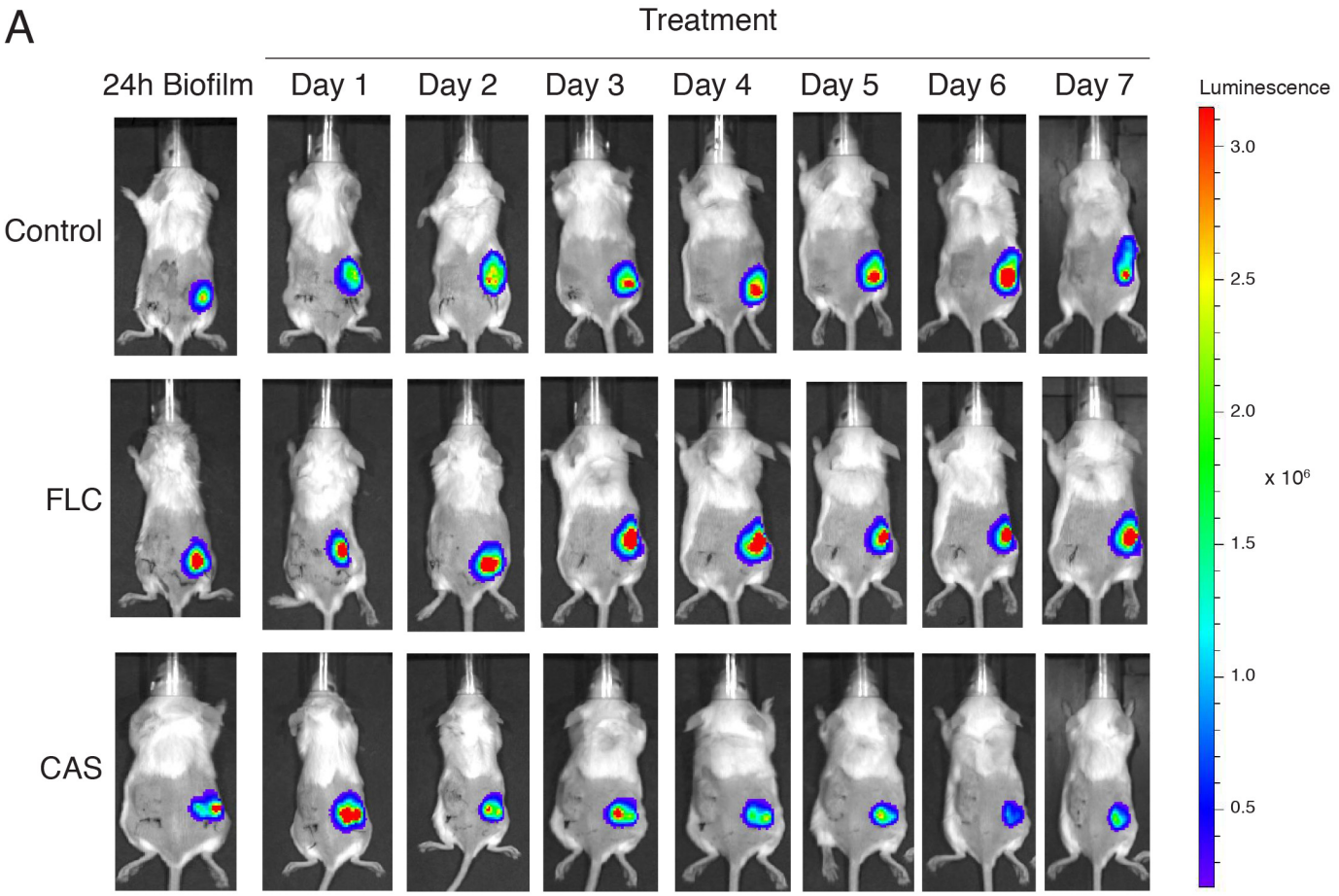
A
Treatment
24h Biofilm
Day 1
Day 2
Day 3
Day 4
Day 5
Day 6
Day 7
Control
FLC
CAS
Luminescence
3.0
2.5
2.0
x 10⁶
1.5
1.0
0.5

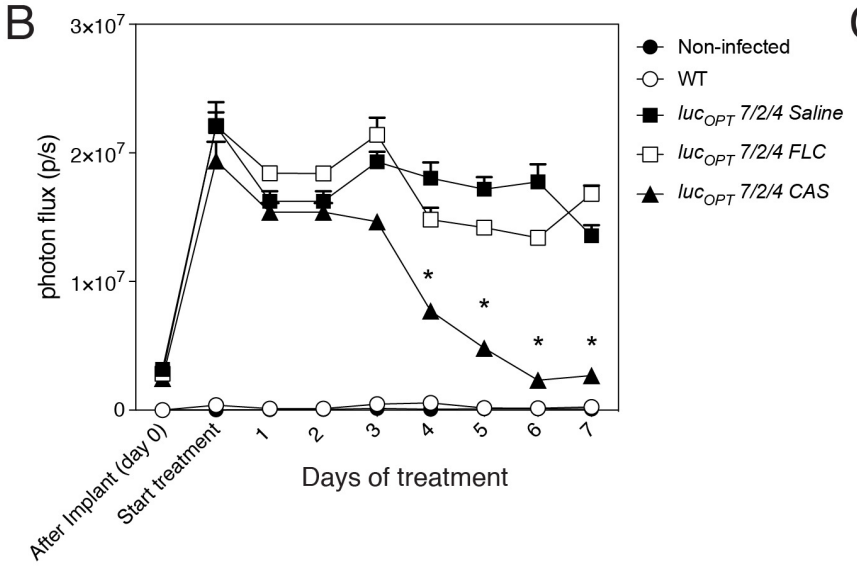
B
3x10⁷
2x10⁷
1x10⁷
0
photon flux (p/s)
After Implant (day 0)
Start treatment
1
2
3
4
5
6
7
Days of treatment
Non-infected
WT
luc_OPT 7/2/4 Saline
luc_OPT 7/2/4 FLC
luc_OPT 7/2/4 CAS

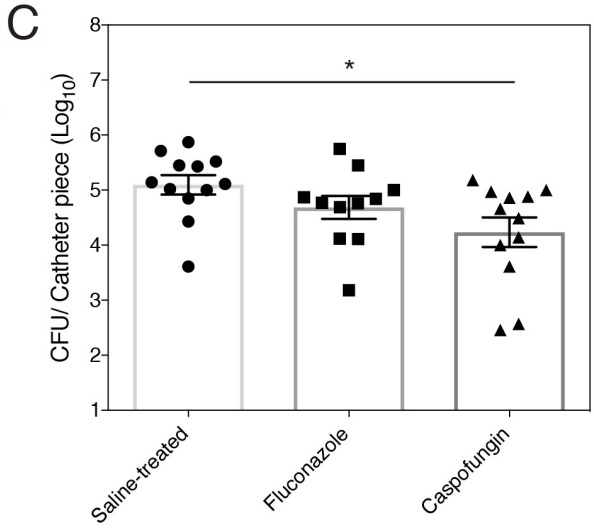
C
CFU/ Catheter piece (Log10)
Saline-treated
Fluconazole
Caspofungin

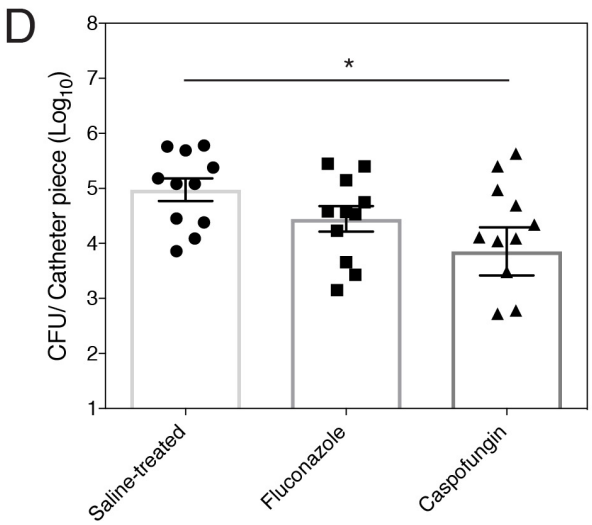
D
CFU/ Catheter piece (Log10)
Saline-treated
Fluconazole
Caspofungin